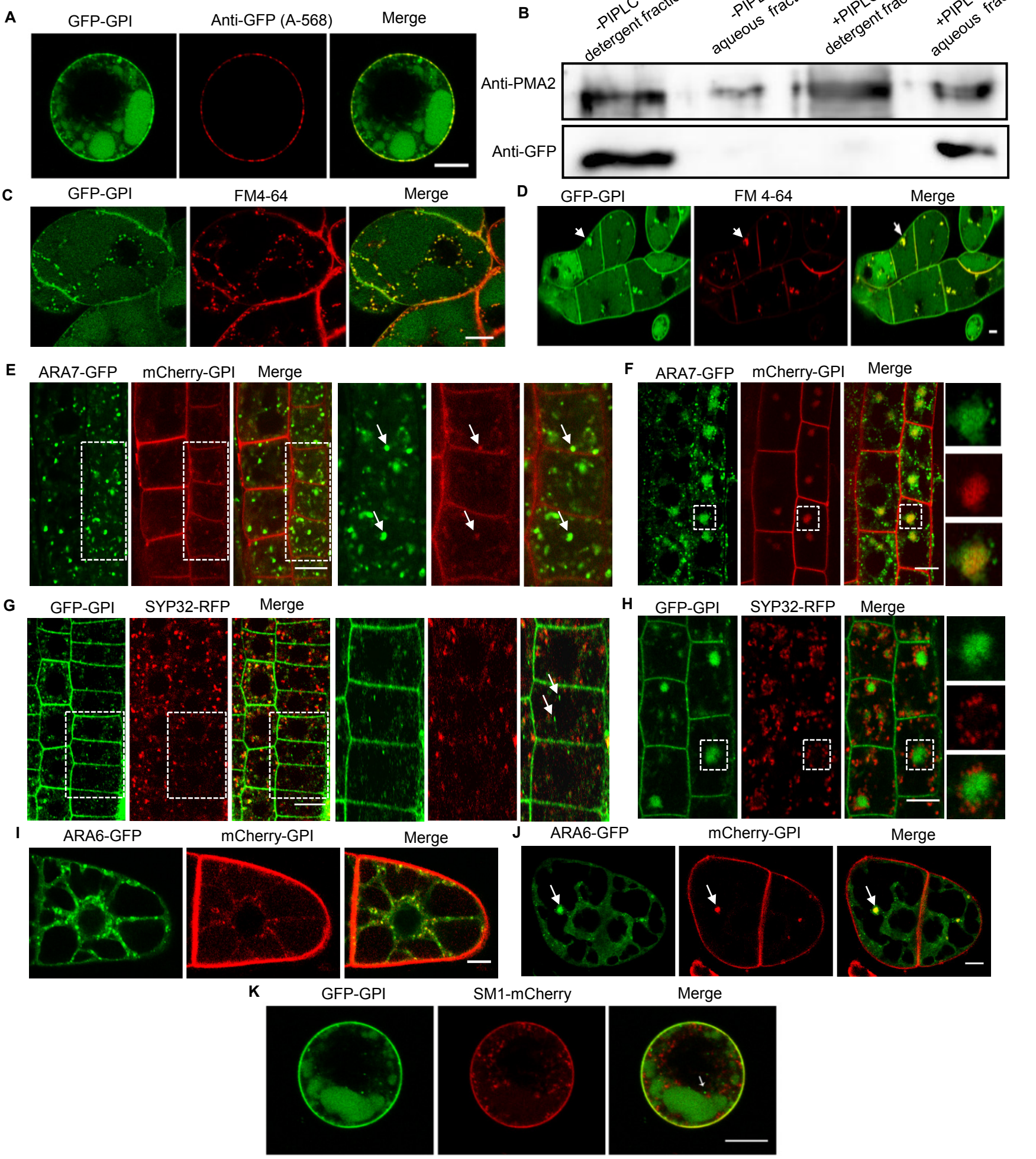

Supplemental Figure-1: Subcellular localization of GPI-anchored proteins.

(A) Surface immunostaining of BY2 protoplasts expressing GFP-GPI with mouse anti-GFP and Alexa-568 labelled goat anti-mouse. **(B)** Protein blot probed with anti-PMA2 and anti-GFP antibodies. Total membrane from GFP-GPI expressing BY2 cells was solubilized in Triton X-114 and phase-partitioned into an aqueous fraction that contains peripheral proteins and a detergent phase that contains integral and lipid -anchored proteins. The detergent phase was treated with PI-PLC (+PIPLC) or with buffer (−PIPLC). After digestion, the reaction mixture was phase re-partitioned into detergent and aqueous phases. Total protein from each fraction was precipitated, run on SDS-PAGE and probed with respective antibodies after blotting. **(C)** GFP-GPI expressing BY2 cells pulsed with 5 μM FM4-64 for 5 min on ice and then chased for 30 min at room temperature. **(D)** GFP-GPI, BY2 cells pulsed with FM4-64 for 5 min and then treated with 50 μM BFA for one hour. White arrow mark a BFA body. **(E**) *Arabidopsis* root epidermal cells expressing ARA7-GFP and mCherry-GPI. Magnified version of boxed area shown in the right. **(F)** BFA treatment (50 μM, 1h) cause agglomeration of ARA7-GFP and mCherry-GPI (inset shows a BFA body in higher magnification). **(G)** *Arabidopsis* root cells expressing SYP32-RFP and GFP-GPI. GFP-GPI vesicles are marked by arrows in the magnified image on the right side. **(H)** SYP32-RFP, GFP-GPI *Arabidopsis* roots treated with BFA (50 μM, 1h). Magnified version of the boxed BFA body is shown in the inset on right side. **(I-J)** BY2 cells double transfected with mCherry-GPI and ARA6-GFP. Control cell **(I)** and cell treated with 50 μM BFA for one hour **(J).** White arrow mark a BFA body. **(K)** GFP-GPI expressing BY2 protoplast transfected with SM1-mCherry. A GFP-GPI vesicle is marked by white arrow. (n, nucleus, Scale bar: 10 μm).

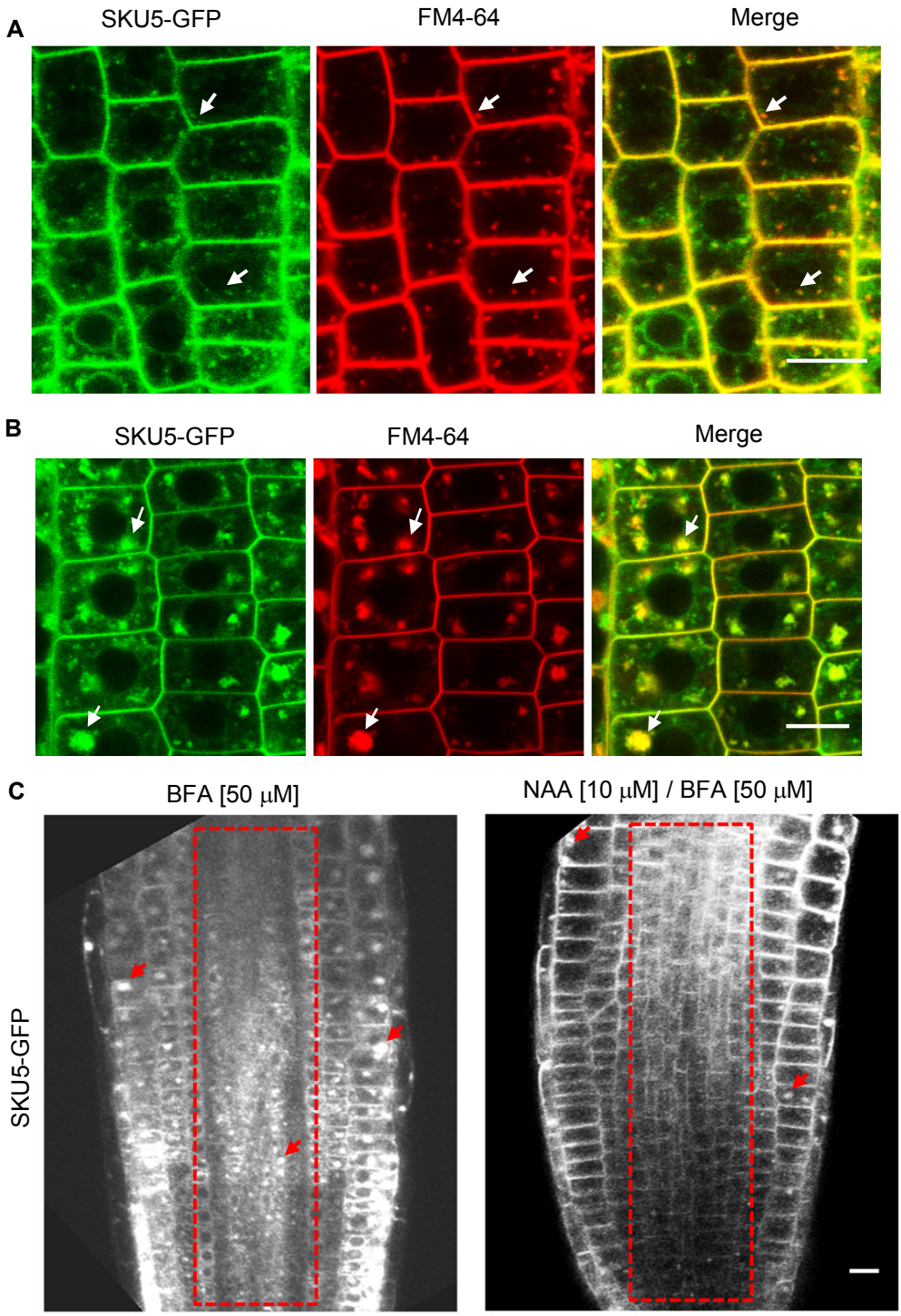

Supplemental Figure 2. Trafficking properties of endogenous GPI-anchored protein SKU5-GFP.

(A) Plants expressing functional SKU5-GFP expressed from the endogenous promoter, pulsed with 5 μM FM4-64 for 5 min on ice, washed and then chased for 10 min at room temperature. Arrows indicate co-localization of SKU5-GFP and endocytosed FM4-64. **(B)** BFA treatment causes aggregation of endocytosed SKU5-GFP together with FM4-64 in epidermal cells (arrows). **(C)** BFA treatment results in clumping of endocytosed SKU5-GFP in all layers of the root (left). In response to NAA pre-treatment, SKU5-GFP accumulates in BFA bodies only in the epidermal cells (right, arrows) but not in the internal layers (boxed area). (Scale bar: 10 μm).

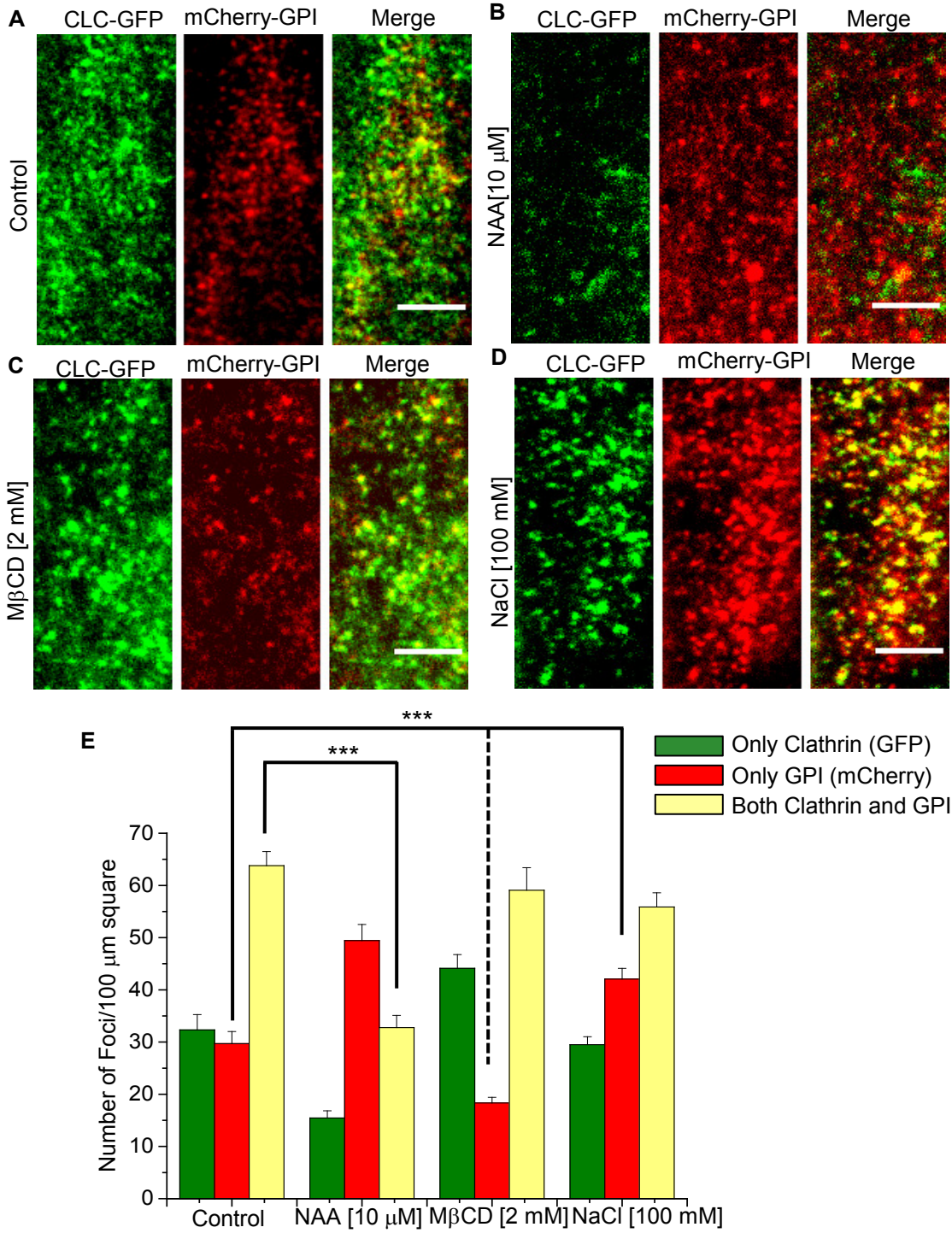

Supplemental Figure 3. VAEM imaging of CLC-GFP and mCherry GPI foci on plasma membrane.

(A-D) *Arabidopsis* root epidermal cells expressing CLC-GFP and mCherry-GPI were imaged by VAEM. Snapshots of first frames of VAEM movies for control plants **(A)** and plants treated with 10 μM NAA **(B),** 2 mM MβCD **(C)** or 100 mM NaCl **(D).** The duration of each treatment was 30 min. **(E)** Quantification of foci containing only CLC-GFP (green bar), only mCherry-GPI (red bar) and both CLC-GFP and mCherry-GPI (yellow bar). The data is collected form10 images for individual treatments across 3 independent experiments. Error bars represent SE of the mean. Asterisks represent p-value < 0.0005 (Student's t-test between groups indicated by brackets) (Scale bar: 5 μm)

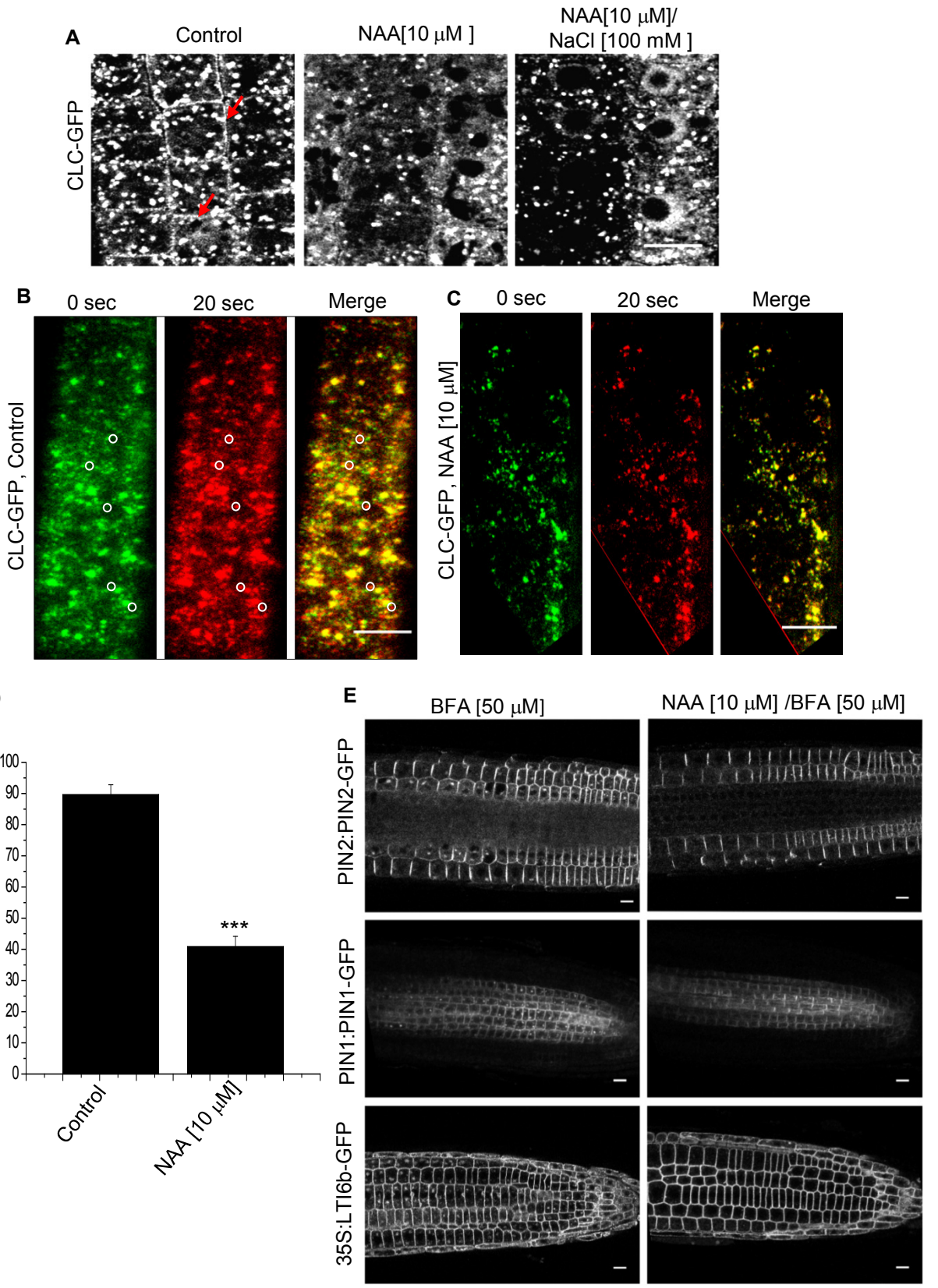

Supplemental Figure 4. Effect of NAA on clathrin-dependent endocytosis.

(A) CLC-GFP at the PM in the absence (left, arrows) or presence (middle) of 10 μM NAA for 30 min. CLC-GFP localization in NAA pre-treated plants which are subsequently co-treated with 100 mM NaCl for 30 min (right). **(B-C)** VAEM imaging of CLC-GFP foci on PM of control plant **(B)** or plant treated with 10 μM NAA for 30 min **(C).** Image taken at 0 sec (green) and 20 sec (red) is superposed to reveal dynamics of the foci over 20 sec. Encircled area in **(B)** marks appearance of new foci. No such foci is formed in NAA-treated plant **(C). (D)** Quantification of CLC-GFP foci abundance on plasma membrane by VAEM imaging. The data are cumulative of two independent experiments with a total of 10 images quantified for each group. Error bars represent SE of the mean. Asterisks represent p-value < 0.0001 (Student's t-test). **(E)** BFA induced aggregation of endocytosed PIN2-GFP, PIN1-GFP and LTI6b-GFP (left) is blocked by NAA pre-treatment (right). (Scale bar: 10 μm).

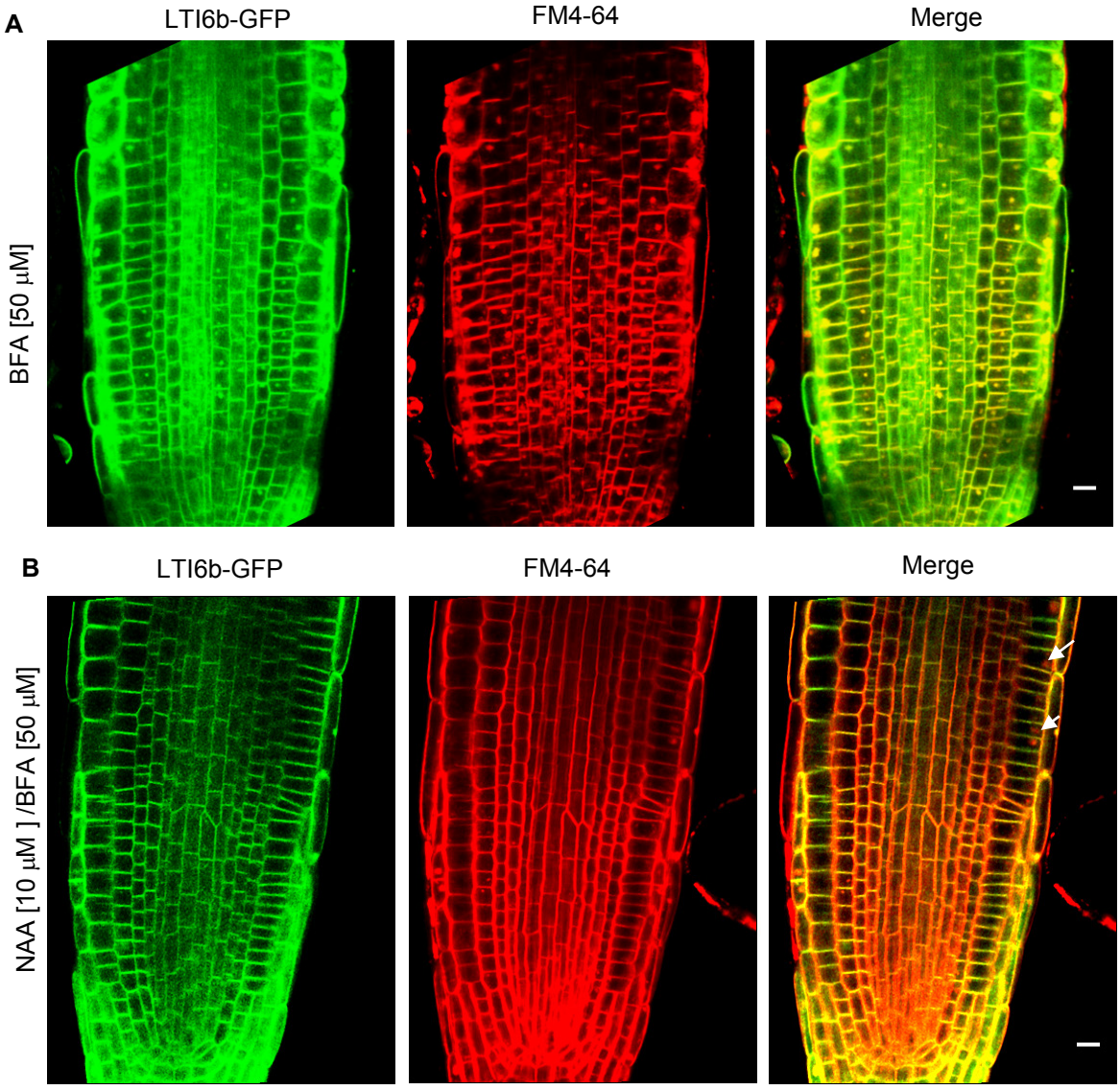

Supplemental Figure 5. Effect of NAA on LTI6b-GFP and FM4-64 uptake.

Uptake and clumping of LTI6b-GFP and FM4-64 in response to BFA treatment **(A)** or NAA + BFA treatment following NAA pre-treatment **(B)**. In presence of NAA pre-treatment, FM4-64 containing BFA bodies are found only in the epidermal layer (White arrow). (Scale bar: 10 μm)

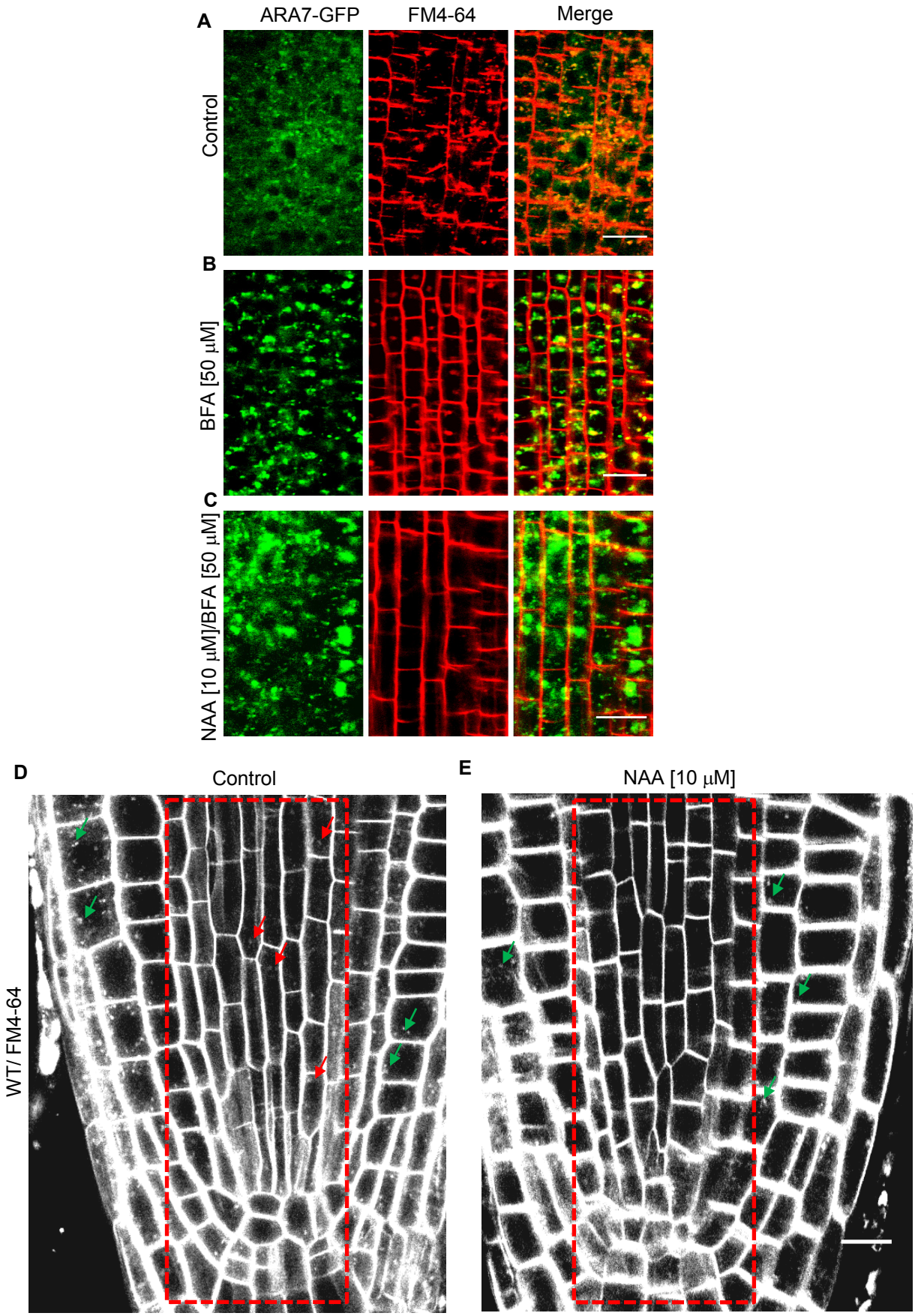

Supplemental Figure 6. NAA blocks endocytosis in stele cells.

(A) ARA7-GFP plants pulsed with 5 μM FM4-64 for 30 min and chased for 1h. **(B)** Uptake and clumping of ARA7-GFP and FM4-64 in response to BFA treatment (50 μM, 1h). Both ARA7-GFP and FM4-64 are present in BFA bodies. In plants pre-treated with NAA (10 μM, 30 min), ARA7-GFP containing BFA bodies still formed but they did not contain any internalized FM4-64 **(C). (D)** WT plants pulsed with 5 μM FM4-64 for 30 min. Internalization of FM in punctate structures can be seen in epidermis (green arrows) and stele (red arrows- dashed box). **(E)** In NAA pre-treated plants uptake is still seen in epidermis (green arrows) but no uptake is seen in stele. (Scale bar: 10 μm)

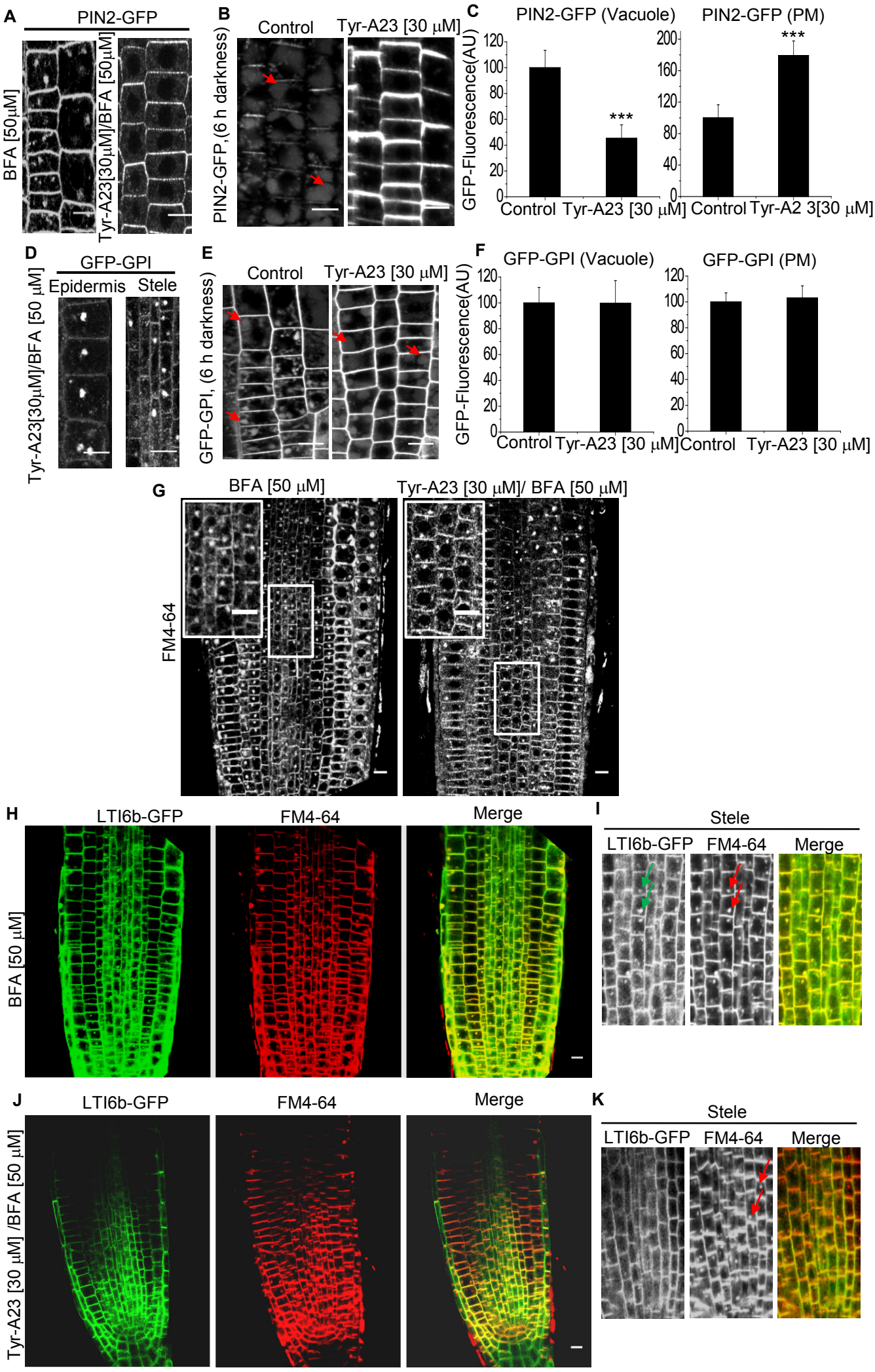

Supplemental Figure 7. Endocytosis in the presence of Tyr-A23.

(A) PIN2-GFP seedlings treated with 50 μM BFA alone (left) or along with 30 μM Tyr-A23 pre-treatment (right). **(B)** Dark treatment (6 h) of PIN2-GFP seedlings in absence (left) and in presence of Tyr-A23 (right). Arrows indicate vacuolar accumulation of PIN2-GFP. **(C)** Quantification of vacuolar (left) and PM associated PIN2-GFP fluorescence in dark-incubated control plants or plants treated with Tyr-A23. **(D)** Endocytosis and BFA induced clumping of GFP-GPI in presence of Tyr-A23 in epidermal cells (left) and stele (right). **(E)** Endocytosis and dark induced accumulation of GFP-GPI in vacuoles of epidermal cells in absence (left) or in presence of Tyr-A23 (right). Arrows indicate accumulation of GFP-GPI in vacuoles. **(F)** Quantification of vacuolar (left) and PM associated GFP-GPI fluorescence in dark-incubated control plants or plants treated with Tyr-A23. **(G)** Uptake and clumping of FM4-64 in response to BFA treatment (left) or withTyr-A23 pre-treatment (right). Insets are magnified version of the outlined area in stele. **(H-K)** Uptake and clumping of LTI6b-GFP and FM4-64 in response to BFA treatment **(H and I)** or with Tyr-A23 pre-treatment **(J and K)**. **(I)** and **(K)** are magnified images of stele region of images **(H)** and **(J).** With Tyr-A23 pre-treatment, FM4-64 containing BFA bodies are found across all the layers while uptake and aggregation of LTI6b-GFP is blocked. Formation of LTI6b-GFP and FM4-64 BFA bodies in stele is marked in BFA treated plants (**I**, green and red arrows). In Tyr-A23 pre-treated plants only FM containing BFA bodies are seen (**K**, red arrows) (Scale bar 10μm). The data presented in **(C)** and **(F)** are from two independent experiments with at least 150 cells quantified per group per experiment. Error bars represent SE of the mean. Asterisks denote p-value <0.0001 (Student's t-test)

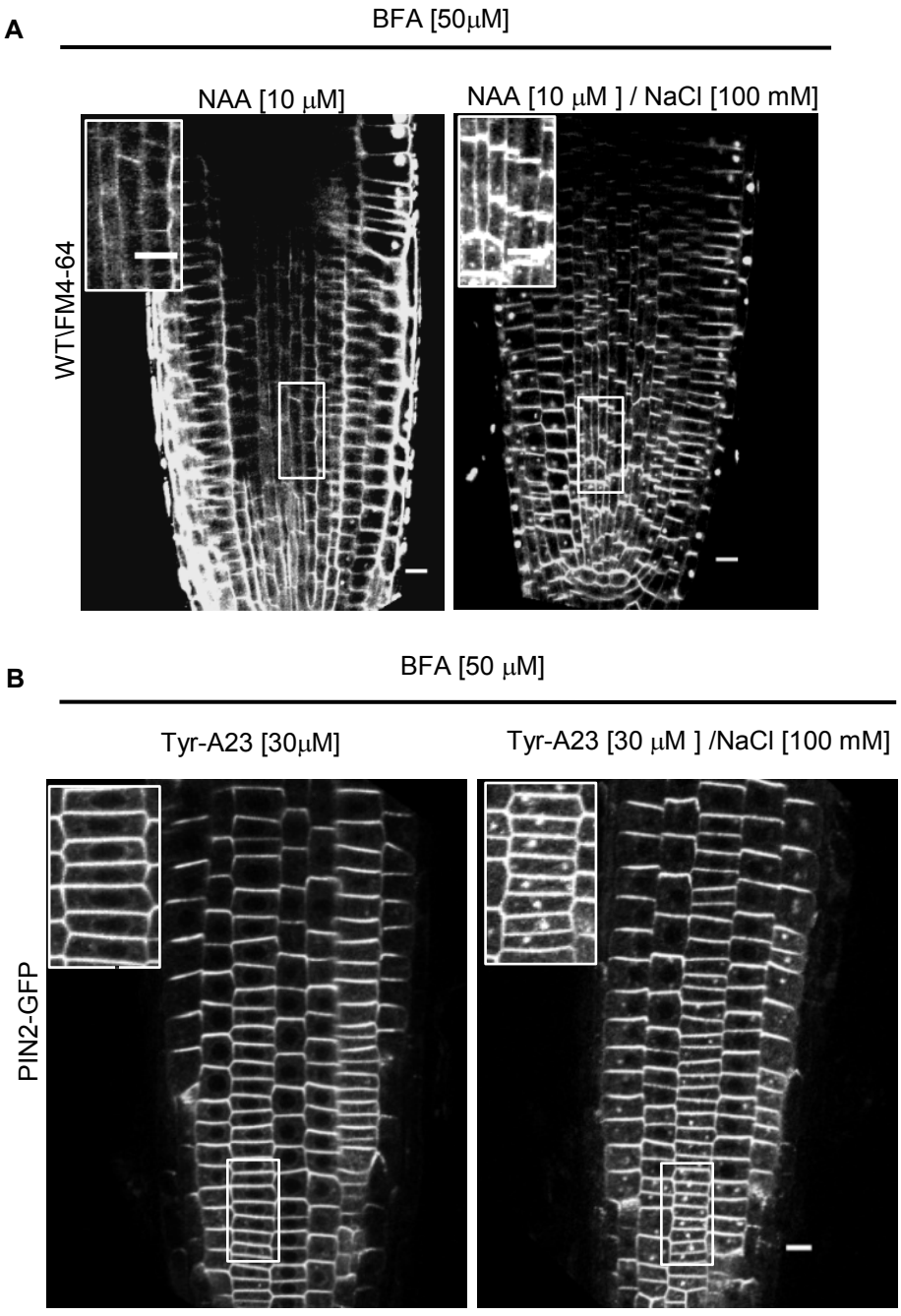

Supplemental Figure 8. Salt induced bulk flow pathway in *Arabidopsis* roots.

(A) Exposure to 100 mM NaCl induces FM4-64 uptake in internal layers of NAA pre-treated WT roots (right, inset). **(B)** NaCl treatment induces uptake of PIN2-GFP in epidermal cells of Tyr-A23 pre-treated roots (right, inset). Insets represent magnified versions of boxed areas. (Scale bar: 10 μm).

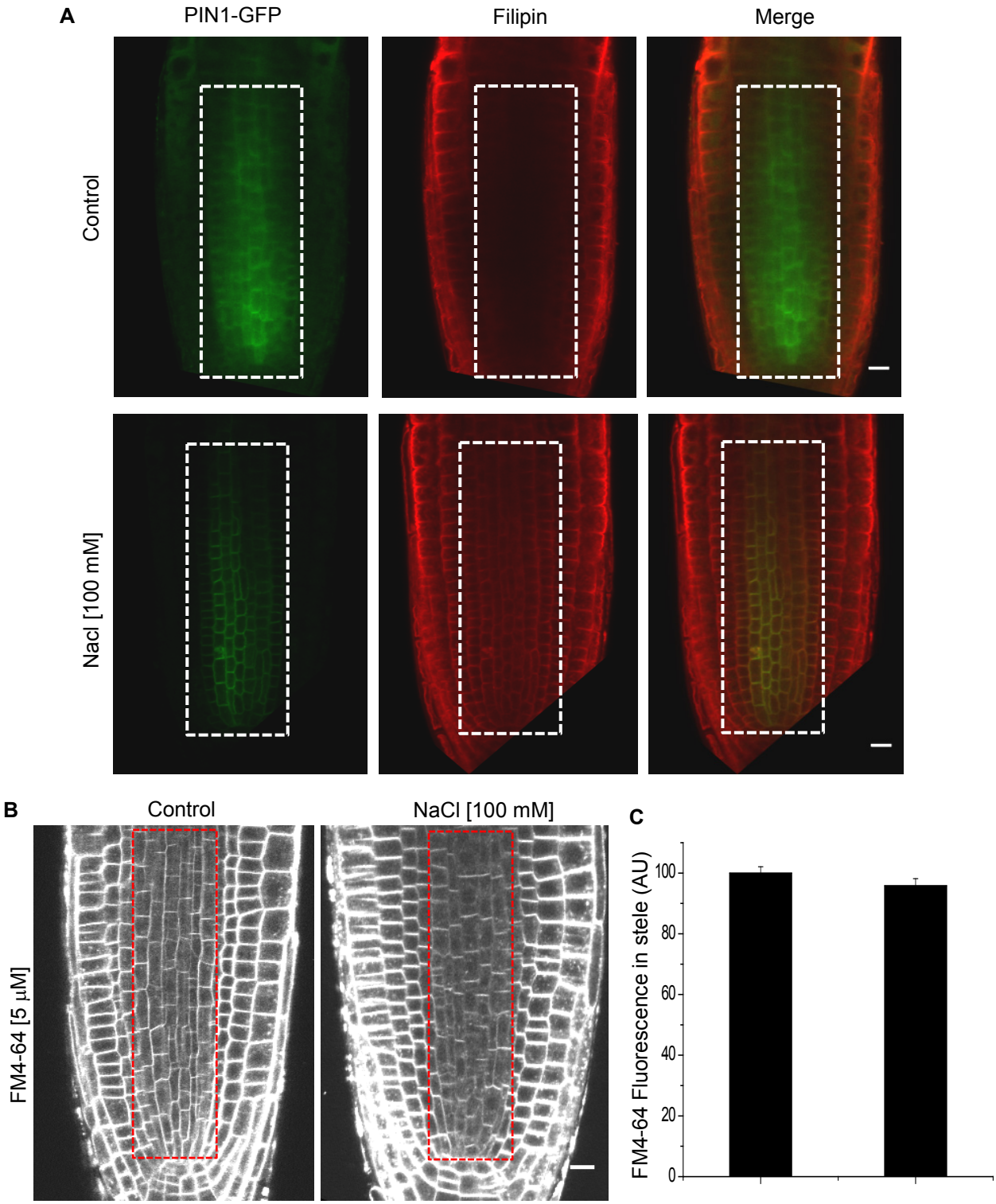

Supplemental Figure 9. Salt induced increase of plasma membrane sterol content of internal cells.

(A) Filipin staining of PIN1-GFP *Arabidopsis* root. Control (top) and salt (100 mM, 1 h) treated plant (bottom) stained with 100 μg/ml filipin for 1 h. Stele is marked by the dashed box. **(B)** Control and salt treated plants stained with 5 μM FM4-64 for 1 h. Stele is marked by the dashed box. **(C)** Quantification of FM labelling of PM of the stele cells of control and salt-treated plants. The result is cumulative of two independent experiments with mean grey value of a total of 245 ROIs for control and 257 ROIs drawn on PM of salt-treated plants quantified. Error bars represent SE of the mean (p-value is 0.41; Student's t-test). (Scale bar: 10 μm)

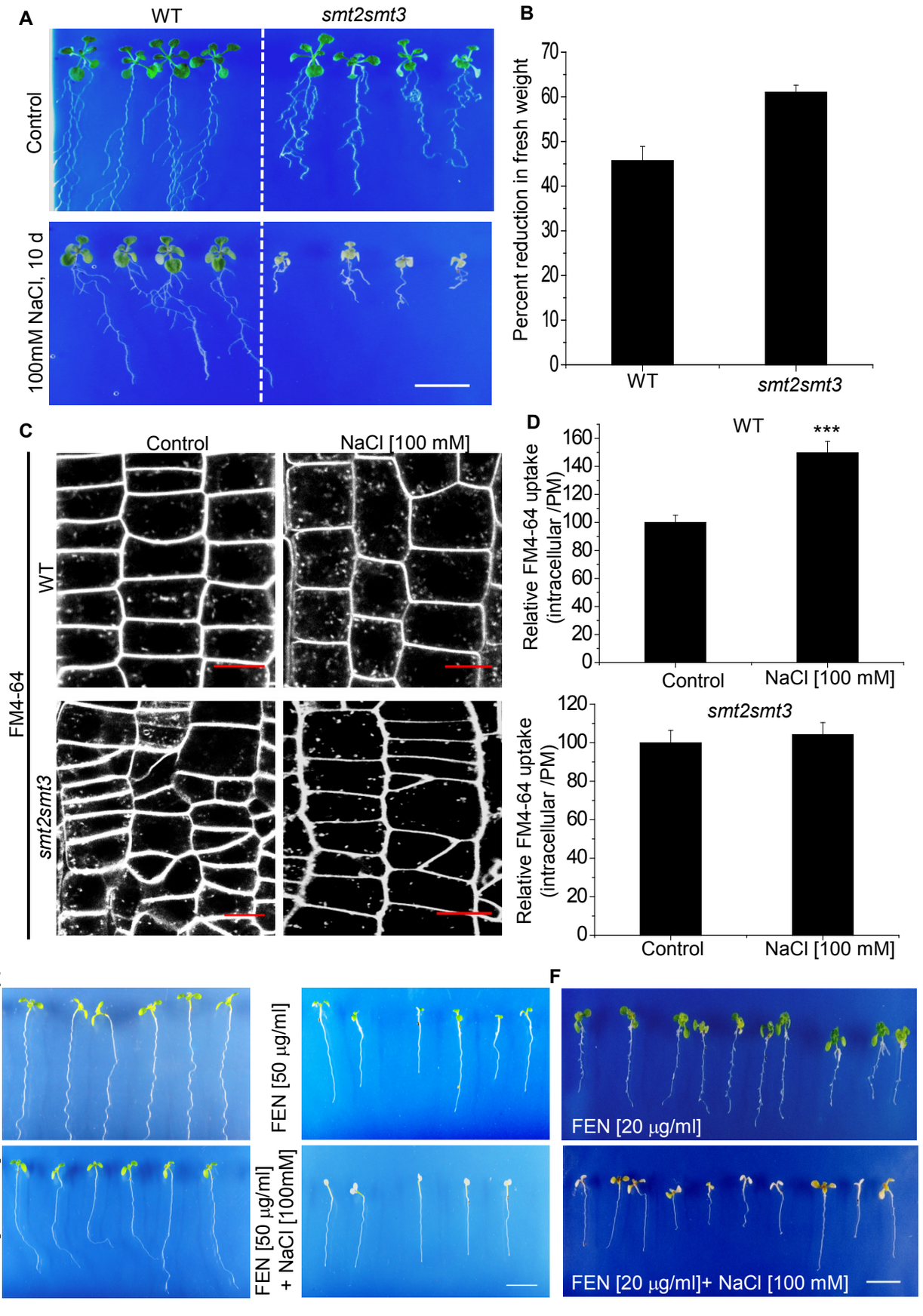

Supplemental Figure 10. Salt sensitivity associated with sterol biosynthetic defects.

(A) Four days old WT and *smt2smt3* plants were transferred to plates containing ½ MS medium (top) or ½ MS medium supplemented with 100 mM NaCl (bottom). After 10 d, salt-treated *smt2smt3* plants turn yellow, while the WT plants remain relatively unaffected. **(B)** Relative reduction of fresh weight of WT and *smt2smt3* plants (normalized to respective control plants) in response to salt stress. **(C-D)** FM4-64 uptake (5 µM, 30 min pulse) in epidermal cells of WT and *smt2smt3* plants under control and salt-stressed condition. The data are cumulative of two independent experiments with 80 cells analyzed per group per experiment. Error bars represent SE of the mean. Asterisks represent p-value <0.0001 (Student's t-test). **(E)** Salt sensitivity (100mM NaCl) of WT plants in absence (left) or in presence of 50µg/ml fenpropimorph (Fen). In presence of fenpropimorph, salt stressed plants die in 4-5 d. **(F)** Fenproimorph-treated (20 µg/ml) plants grown in absence (top) or in presence (bottom) of 100 mM NaCl for 10 d. (Scale bar: 1 cm in **A, E, F** and 10 µm in **C**).

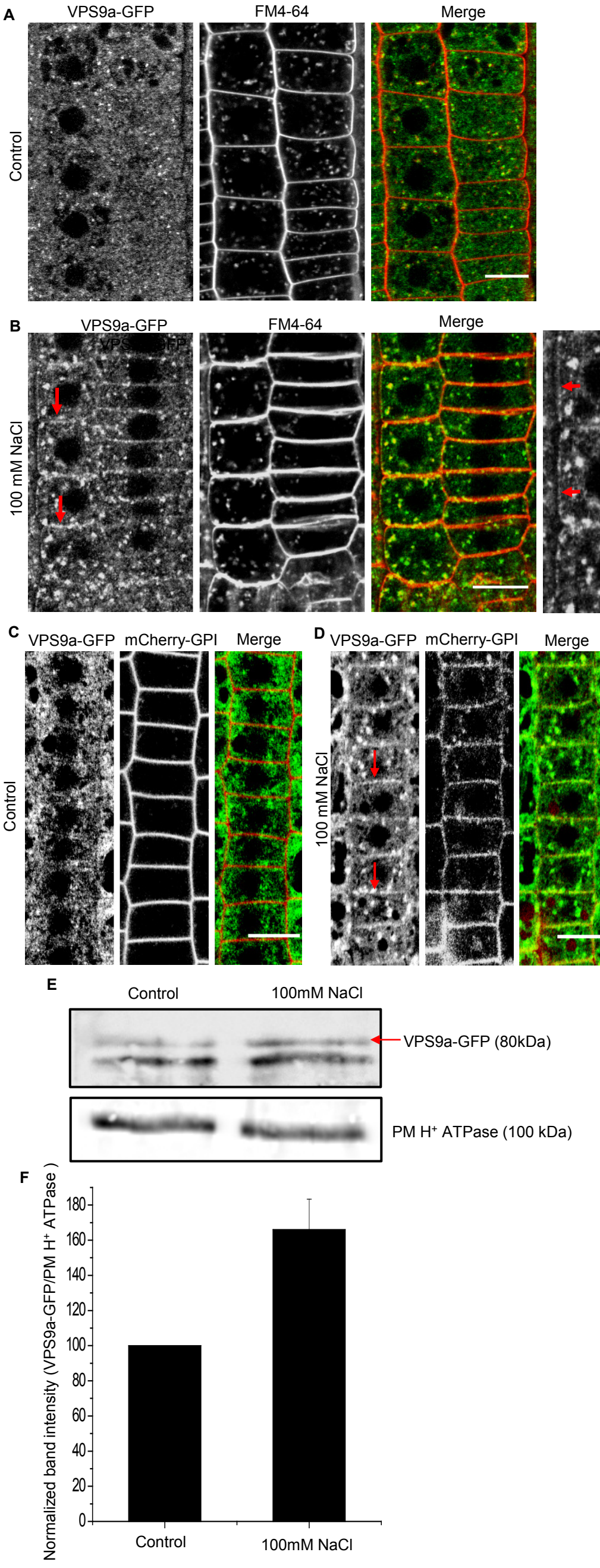

Supplemental Figure 11. Association of VPS9a-GFP with plasma membrane under salt-stress.

(A-B) VPS9a-GFP localization in root epidermal cells in FM4-64 stained control plants **(A)** or salt-stressed (100 mM, 45 min) plants **(B).** Inset in **(B)** is magnified version of the GFP channel image. Arrows indicate PM association of VPS9a-GFP. **(C-D)** Root epidermal cells of plants expressing VPS9a-GFP and mCherry-GPI. Control plants **(C)** or salt-stressed (100 mM, 30min) plants **(D).** Arrows in **(D)** indicate PM association of VPS9a-GFP. **(E)** Immunoblotting of total membrane fraction of VPS9a-GFP plants in control or salt-stressed conditions. The blot is probed with Anti-GFP as proxy for VPS9a-GFP and Anti-PM H^+ ATPase as loading control. The Anti-GFP recognizes multiple bands in the blot, of which the 80kDa band is of the calculated molecular weight of full length VPS9a-GFP (Arrow). **(F)** VPS9a-GFP band intensities normalized with PM H^+ ATPase band intensity in control and salt-stressed (100 mM, 30min) plants. The data represented are from two independent repeats. (Error bar represents standard deviation). (Scale bar: 10 μm).

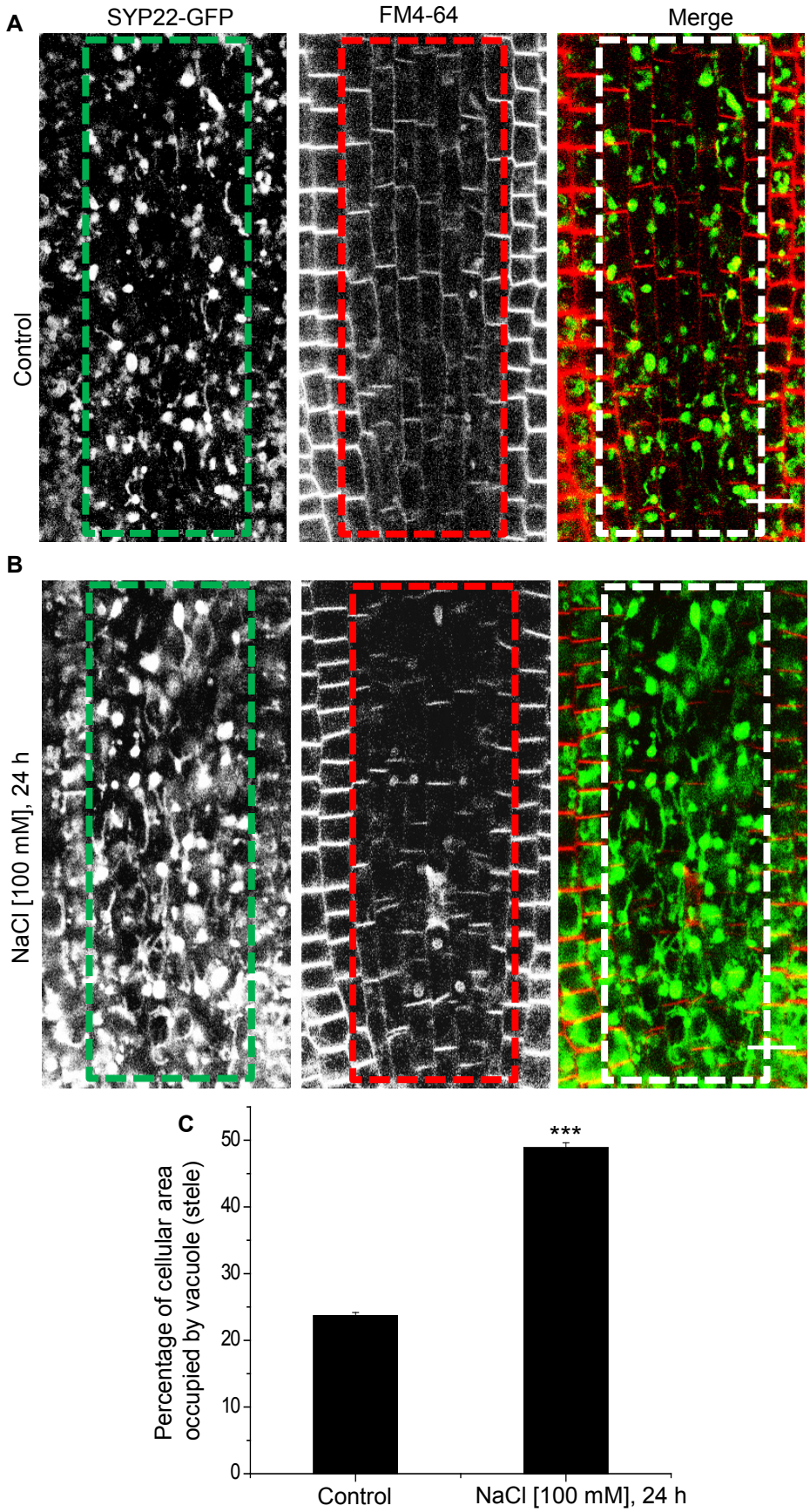

Supplemental Figure 12. Expansion of vacuolar structures in stele in response to salt-stress.

Three days old *Arabidopsis* seedlings expressing SYP22-GFP were incubated either on ½ MS (control) **(A)** or ½ MS +100 mM NaCl for 24 h **(B)**. In stele of salt treated root, expansion of SYP22-GFP labelled vacuolar structures can be seen. Cell outline is marked by short pulse (15 min) of FM4-64. **(C)** Quantification of cellular area occupied by SYP22-GFP labelled vacuoles under control conditions or after 24 h salt stress. Bars represent weighted mean of percentage of cellular area occupied by vacuoles ± SE of the mean. Asterisks indicate p-value <0.0001(Student's t-test). Plotted data is a sum of two independent experiments with at least 150 cells quantified per treatment. (Scale Bar: 10 μm)